PHYSICAL REVIEW C VOLUME 22, NUMBER 3 SEPTEMBER 1980

Shape parametrization for liquid-drop studies

S. Trentalange and S. E. Koonin
W. K. Kellogg Radiation Laboratory, California Institute of Technology, Pasadena, California 91125

A. J. Sierk*
Theoretical Division, Los Alamos Scientific Laboratory, University of California, Los Alamos, New Mexico 87545
and W. K. Kellogg Radiation Laboratory, California Institute of Technology, Pasadena, California 91125
(Received 6 November 1979)

We present a new method for defining axially symmetric shapes which is particularly appropriate for describing elongated and multineck configurations. This shape parametrization is used to describe the static properties of incompressible, charged liquid drops. In particular, we calculate the properties of binary-fission saddle points and compare these with results using other methods. We also present the geometrical properties and normal mode analyses of the two- and three-necked saddle-point families.

[NUCLEAR REACTIONS, FISSION Liquid-drop model; new shape parametrization; calculated binary-fission saddle points, multinecked saddle points, normal modes of saddle-point shapes; Werner-Wheeler approximation.]

I. INTRODUCTION

The liquid-drop picture is a useful conceptual framework for discussing nuclear collective motion.[1-8] The three key quantities in this context are the potential energy, rate of energy dissipation, and collective kinetic energy, all expressed as functionals of the nuclear shape and its time derivatives. Although a finite-difference treatment of the problem is possible,[9] most previous studies have resorted to the far simpler approach of parametrizing the nuclear shape in terms of a few dynamical variables and making assumptions about the flow of matter in the nuclear interior. The utility of a given parametrization depends on both how closely it can approximate the shapes through which the real system evolves and on how conveniently the three key quantities can be evaluated for any given shape. Most previous parametrizations are able to describe accurately the *static* properties of binary (single-necked) configurations. However, many suffer from the defect of being difficult to generalize (i.e., add more parameters), and all are restricted to *only* binary shapes. This last feature eliminates the possibility of studying ternary fission, which might be the preferred mode of breakup for very heavy systems. In addition to these static limitations, certain parametrizations are known to lead to unphysical shapes in dynamical studies of heavy-ion collisions.[10-12]

This paper is the first in a series reporting studies with a new parametrization of axially symmetric shapes designed to at least partly resolve some of the problems mentioned above. By expanding the square of the drop's cylindrical radius in Legendre polynomials of the dimensionless distance along the symmetry axis, we obtain a flexible, easily generalizable parametrization in which the potential energy and inertial coefficients are comparatively easy to evaluate. In this report, we focus on the static properties of nonrotating, mass-symmetric systems. Section II presents our new parametrization, and its relation to those used previously. Section III is a discussion of the static equations of the nuclear liquid drop. We compare the properties of binary-fission saddle points calculated with our new parametrization to those of earlier studies in Sec. IV, and consider the properties of two less familiar families of saddle points, those with two and three degrees of instability. In Sec. V we discuss our results and present our conclusions. Subsequent papers will deal with fission and heavy-ion collisions and an extension to mass-asymmetric systems.

II. SHAPE PARAMETRIZATIONS

For shapes not too different from a sphere, a spherical-harmonic expansion of the radius vector[1,3,4,13]

$$R(\theta,\varphi)=\frac{R_0}{\lambda}\left[1+\sum_{n,m}\beta_{nm}Y_{nm}(\theta,\varphi)\right] \tag{1}$$

provides a good representation. Here Y_{nm} is a spherical harmonic, R_0 is the radius of the unperturbed sphere, $\lambda(\beta)$ is a normalization constant which ensures volume conservation, and the $\{\beta_{nm}\}$ are the parameters describing the shape. (This function is often used in the axially sym-

metric form where $\beta_{nm}=0$ for $m\neq 0$.) This parametrization has the advantage of allowing a simple check of convergence properties by varying the maximum value of n included in the truncated sum. However, it is not able to adequately represent the more deformed saddle-point shapes of light nuelci, or a more complex shape whose radius may be a double-valued function of θ. A generalization of Eq. (1) which allows accurate description of somewhat more elongated configurations is an expansion about spheroidal shapes.[14,15]

The deficiencies of Eq. (1) make it attractive to use an alternative description in terms of cylindrical coordinates. Thus, the cylindrical radius of the surface ρ_s is expressed as a function of z and φ, the remaining two coordinates. Most studies using parametrization of this type have been confined to axially symmetric shapes, so that ρ_s is independent of φ. One example of these is[5,16-18]

$$\rho_s^2(z)=(c^2-z^2)(\alpha_1+\alpha_2 z+\alpha_3 z^2), \tag{2}$$

where c and the $\{\alpha_i\}$ are the parameters. The form of Eq. (2) emphasizes its relation to a spheroid. This parametrization is quite useful, but is somewhat restricted in its ability to describe shapes near scission and near the contact point in heavy-ion collisions.

Another method of describing elongated shapes is to use two spheroids, either separated, overlapping, or smoothly joined, with a function describing a neck region between them. One parametrization of this sort uses separated spheroids with a fourth order polynomial in z for the region between their centers. A parametrization extensively used which is able to describe two spheroids separated or in contact as well as fissioning nuclei is the three-quadratic-surface parametrization.[6] Here the ends of the shape are spheroids, joined smoothly by a third spheroid or by a hyperboloid of one or (for separated systems) two sheets. Again, this parametrization is rather difficult to generalize.

One attractive possibility which has not been explored is to generalize Eq. (2) to an arbitrary number of parameters $\{\alpha_i\}$. Equivalently, we propose a truncated Legendre-polynomial expansion for the axially symmetric shapes

$$\rho_s^2(z)=R_0^2\sum_{n=0}^{N'} a_n P_n\left(\frac{z-\bar{z}}{z_0}\right), \tag{3}$$

where $\bar{z}$ is the coordinate of the midpoint between the two ends and $2z_0$ is the distance between the end points. Since the arguments of the Legendre polynomials vary between -1 and 1, we are able to take advantage of orthogonality and other properties of the Legendre functions. For the remainder of this paper, we consider only reflection-symmetric shapes, for which $\bar{z}=0$, and $a_n=0$ for n odd. (The more general case of asymmetric shapes will be discussed in a later paper.) Thus we define the dimensionless function

$$u(x)\equiv\rho_s^2(z)/R_0^2=\sum_{\substack{n=0\\ \text{even}}}^{2N} a_n P_n(x), \tag{4}$$

where $x\equiv z/z_0$ varies from -1 to 1, and $2N$ is the maximum order of Legendre polynomial considered. Figure 1 illustrates how $u(x)$ is related to the shape it describes.

The parameters a_n and z_0 of Eq. (4) are not all independent. Requiring that $u(x)=0$ at $x=\pm 1$ ($z=\pm z_0$, the ends of the drop) implies that

$$a_0=-\sum_{\substack{n=2\\ \text{even}}}^{2N} a_n, \tag{5}$$

while volume conservation requires

$$z_0=2R_0/3a_0. \tag{6}$$

Equations (5) and (6) eliminate a_0 and z_0 as independent variables, leaving N separate parameters $\{a_2, a_4, \ldots, a_{2N}\}$ describing a reflection-symmetric shape. Note that because of Eq. (5), Eq. (4) may be rewritten as

$$u(x)=\sum_n a_n[P_n(x)-1], \tag{7}$$

where the shorthand notation $\sum_n$ indicates $\sum_{n=2}^{2N}$ with n even.

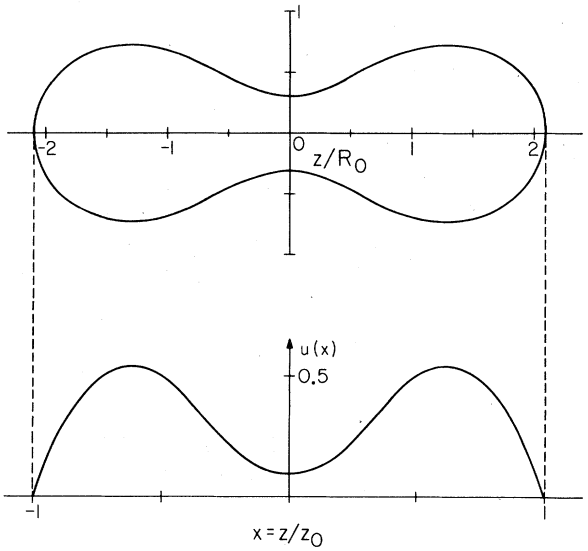

FIG. 1. Upper portion: Intersection of the surface defining the $x=0.5$ binary saddle-point shape with a plane through the axis of symmetry. Lower portion: $u(x)$ for the same shape with the x scale magnified to align $x=\pm 1$ with the ends of the shape above.

Since the vibrational normal modes of the spherical nonrotating drop are pure spherical-harmonic distortions,[4,13] it is of interest to express the relation between the $\{\beta_{nm}\}$ of Eq. (1) and the $\{a_n\}$ of Eq. (4) for axially symmetric shapes not greatly distorted from a sphere. If we express Eq. (1) for an axially symmetric and mass-symmetric shape in terms of Legendre polynomials of polar angle instead of spherical harmonics, we may write

$$R(\theta)=\frac{R_0}{\lambda}\left[1+\sum_n b_n P_n(\cos\theta)\right], \tag{8}$$

where $b_n=(2n+1/4\pi)^{1/2}\beta_{n0}$. If we assume $b_n \ll 1$ for all n, using

$$\rho_s^2(z)=R^2(\theta)(1-\cos^2\theta) \tag{9}$$

and $\cos\theta=z/R(\theta)$, we find to first order in the b's:

$$a_2=-\tfrac{2}{3}+\tfrac{2}{3}b_2-\tfrac{4}{3}\sum_{n\geq 4} b_n, \tag{10a}$$

$$a_n=2b_n \text{ for } n>2. \tag{10b}$$

Thus, an interesting property of our parametrization is that *any* small distortion of a sphere involves a change in a_2, while a normal-mode distortion of higher order than quadrupole involves only one other nonzero a_n.

III. STATIC EQUATIONS FOR THE NUCLEAR LIQUID DROP

We work in dimensionless units, where the unit of length is R_0, the radius of the spherical nucleus; the unit of mass is M_0, the mass of the nucleus; and the unit of energy is $E_s^{(0)}$, the surface energy of the spherical nucleus.

The dimensionless fissility parameter x which measures the relative importance of the Coulomb energy in a given system, is defined as

$$x\equiv\frac{E_c^{(0)}}{2E_s^{(0)}}, \tag{11}$$

where

$$E_c^{(0)}=\frac{3}{5}\frac{Z^2e^2}{R_0}$$

is the Coulomb energy of a spherical nucleus with charge Ze. Similarly, the dimensionless rotational energy parameter y is defined as

$$y\equiv E_r^{(0)}/E_s^{(0)}, \tag{12}$$

where

$$E_r^{(0)}=\frac{L^2}{2I_0}=\frac{5}{4}\frac{L^2}{M_0R_0^2} \tag{13}$$

is the rotational energy of a rigidly rotating sphere with angular momentum L and moment of inertia $I_0=\frac{2}{5}M_0R_0^2$. With these definitions, we may express the deformation potential energy relative to that of the nonrotating sphere as

$$\begin{aligned}\zeta&=(E-E_s^{(0)}-E_c^{(0)})/E_s^{(0)}\\&=B_s-1+2x(B_c-1)+yB_R,\end{aligned} \tag{14}$$

where $B_s=E_s/E_s^{(0)}$, $B_c=E_c/E_c^{(0)}$, and $B_r=E_r/E_r^{(0)}$ are all functionals of the nuclear shape, and hence depend upon the parameters $\{a_n\}$. Appendix A contains explicit formulas for B_s, B_c, B_r and their derivatives with respect to the $\{a_n\}$.

The conditions for an equilibrium shape are

$$\frac{\partial\zeta}{\partial a_n}=0=\frac{\partial B_s}{\partial a_n}+2x\frac{\partial B_c}{\partial a_n}+y\frac{\partial B_R}{\partial a_n}, \quad n=2,4,\ldots,2N. \tag{15}$$

We solve these equations iteratively with a vector version of Newton's method. Given a set of coordinates $\{a_n\}$, a new set $\{a_n'\}$ is computed from

$$a_n'=a_n-\sum_m [K^{-1}]_{nm}\frac{\partial\zeta}{\partial a_m}(a), \tag{16}$$

where $K_{nm}=\partial^2\zeta/\partial a_n\partial a_m$ is the symmetric curvature matrix. In practice we use the coordinates of a known equilibrium shape as starting values for a drop with an incremented value of x or y.

To determine the degree of instability of a saddle-point shape, we found the normal-mode frequencies $\{\omega_n\}$. These are solutions to the eigenvalue problem[6]

$$\sum_m (K_{nm}-\omega^2M_{nm})V_m=0, \quad n=2,4,\ldots,2N \tag{17}$$

where V is the normal-mode eigenvector, M is the inertia tensor, and both M and K are evaluated at the saddle point. We therefore find the $\{\omega_n\}$ as the eigenvalues of the matrix $M^{-1}K$. Appendix A contains the expressions we use to compute the inertia tensor in the Werner-Wheeler approximation to incompressible, irrotational flow.

IV. SADDLE-POINT SHAPES

For the nonrotating liquid drop ($Y=0$), the simplest family of equilibrium shapes is the spherical ground state. This shape is a local minimum in the potential-energy surface for $x<1$, and is therefore stable. The familiar binary saddle-point family exists at a higher energy than the ground state. The saddle-point shape for $x=0$ is two tangent spheres. As x increases, a neck forms and the shape becomes progressively more cylinderlike, spheroidal, and spherical, where it crosses the end point of the spherical ground-state family at $x=1$ and the

TABLE I. Binary saddle-point properties. Maximum and minimum extension and energy in natural units for selected binary saddle points calculated using three different parametrizations. The left-hand column contains the results of a nine-term spherical harmonic expansion (Ref. 4), the center column gives the results of the three-quadratic-surface shape description (Ref. 6), and the right-hand column gives the results of the present work using Eq. (4) with $N=8$.

	Cohen and Swiatecki (9 parameters)			Three quadratic surfaces (3 parameters)			Present work (8 parameters)		
x	R_{max}	R_{min}	ζ	R_{max}	R_{min}	ζ	R_{max}	R_{min}	ζ
0.1				1.7602	0.0253	0.233 63	1.7610	0.0218	0.233 71
0.2				1.8576	0.0778	0.202 17	1.8544	0.0637	0.202 14
0.3	1.9624	0.0730	0.169 24	1.9320	0.1275	0.168 14	1.9306	0.1184	0.167 91
0.4	2.0016	0.1286	0.132 84	1.9972	0.1781	0.132 36	1.9931	0.1715	0.131 90
0.5	2.0623	0.2013	0.095 35	2.0567	0.2357	0.095 27	2.0493	0.2291	0.094 64
0.6	2.0977	0.2993	0.056 95	2.1003	0.3167	0.057 47	2.0890	0.3094	0.056 74
0.7	1.8906	0.5352	0.022 36	1.9142	0.5368	0.022 93	1.8893	0.5354	0.022 37
0.8	1.5025	0.7493	0.005 91	1.5185	0.7490	0.006 05	1.5023	0.7540	0.005 91
0.9	1.2353	0.8831	0.000 71	1.2411	0.8825	0.000 73	1.2354	0.8829	0.000 71

binary-fission barrier disappears. (The binary saddle-point continues as an increasingly oblate shape for $x>1$.) For $x\leq 1$ this family has one degree of instability corresponding to the fission degree of freedom. For $x\leq 0.396$ there is a second instability corresponding to a mass-asymmetric motion.[4,6,14] In the present study, we consider only reflection-symmetric modes.

Besides this well-studied binary sequence, there exist families of saddle points at higher

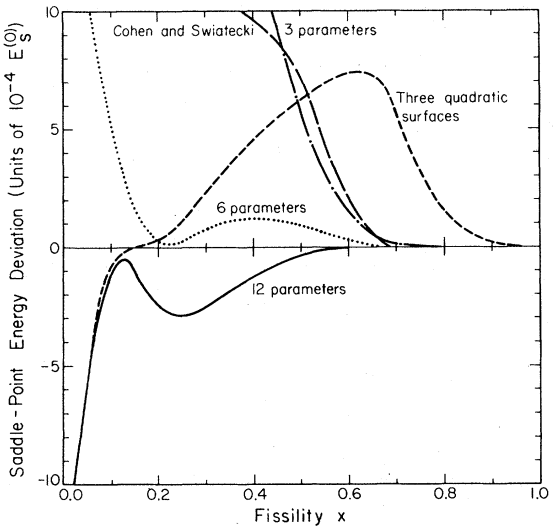

FIG. 2. Deviation of calculated binary saddle-point energies from the results using Eq. (4) with $N=8$. "Cohen and Swiatecki" refers to Ref. 4 which used a nine-term expansion in spherical harmonics. "Three quadratic surfaces" refers to the results of Ref. 6; "N parameters" refers to the present calculations using different values of N. A positive deviation indicates a poorer approximation to the correct saddle-point shape. (See text for explanation.)

energies with greater degrees of instability and which, for $x=0$, reduce to a linear array of tangent spheres.[19] In addition, there can be a variety of relationships among the more complex shapes. The ternary and quaternary families, for example, do not cross each other as the simpler shapes do, but exhibit a confluence, or limiting point, at a value of x less than 1.

We begin by comparing the properties of the nonrotating binary saddle points (the so-called y family of shapes) in various parametrizations, as calculated by Cohen and Swiatecki using the spherical harmonic expansion (8) with nine parameters,[4] as calculated by Nix with the three-parameter three-quadratic-surface parametrization,[6] and as calculated using our new parametrization Eq. (4) with eight parameters ($N=8$). In Table I we show the energy and the minimum and maximum spherical radii of the saddle-point shape for several values of x. In Fig. 2 we plot the energies of the spherical-harmonic and three-quadratic-surface saddle points relative to those of our Legendre-polynomial expansion with $N=8$. The results using our parametrization with $N=3$, 6, and 12 are also shown. Under certain conditions, satisfied here, the energy computed for a saddle-point shape is an upper limit to the exact solution. These conditions require the parametrization to be flexible enough to describe shapes on both sides of the pass in the neighborhood of the true saddle point. In comparing the $N=8$ version of our new parametrization to the earlier calculations, we see that both it and the nine-parameter spherical-harmonic expansion are a better representation than the three-parameter three-quadratic-surface shapes for the cylinderlike saddle points with $x\gtrsim 0.7$. Moreover, it gives the lowest energy for x in the range

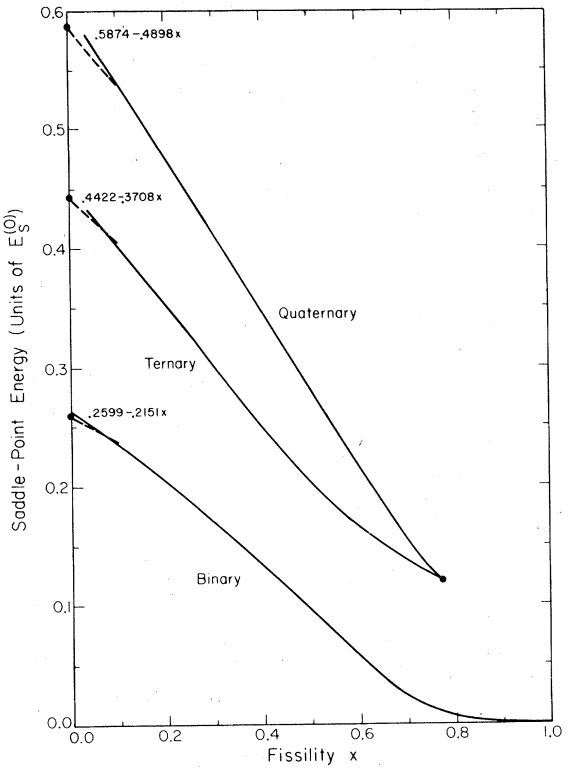

FIG. 3. The energies of the three saddle-point families as a function of x. The dotted and dashed lines near the $x=0$ axis indicate the known values for two, three, and four tangent spheres.

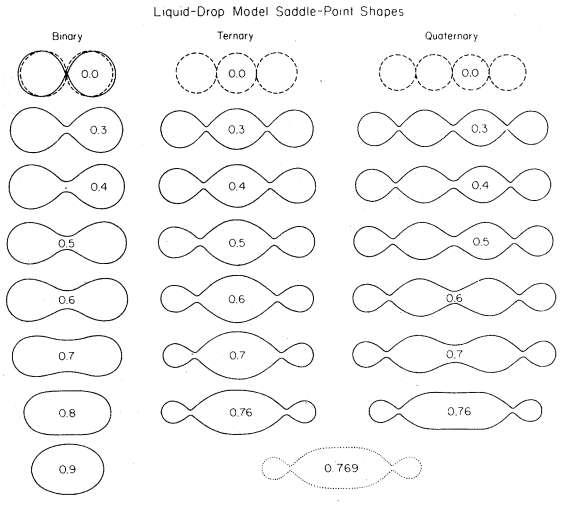

FIG. 4. Binary, ternary, and quaternary saddle-point shapes for selected values of x, indicated by the number inside the shape. Since we could not calculate the ternary-quaternary confluence point directly, the coordinates of this shape at $x=0.769$ were found by extrapolating the shape coordinates of the two- and three-necked families to where they coincided.

0.15–0.70, although the three-quadratic-surface form is superior for $x \lesssim 0.15$. This is so since it can easily represent a neck with high curvature and small radius, a situation which requires very short wavelength (large n) terms in Eq. (4). The convergence of our parametrization with N illustrated in Fig. 2 shows that $N=3$ is sufficient for $x \gtrsim 0.8$, $N=6$ is appropriate for $x \gtrsim 0.65$, and $N=12$ is a substantial improvement over $N=8$ for $x \lesssim 0.55$.

Multi-necked families of equilibrium shapes were first considered in some detail by Ref. 19, in which axially symmetric, but otherwise unconstrained, shapes were used. In Fig. 3, we show our results as a function of x, for the binary, ternary, and quaternary saddle-point energies. Our results agree with those of Ref. 19 to the extent to which they can be compared, although the calculated energies are somewhat higher than the known values for very small x because of the difficulty in representing tangent spheres by means of the Legendre-polynomial expansion with small N.

The shapes of the three saddle-point sequences are shown in Fig. 4 for selected values of x. The evolution of the ternary familty is similar in many respect to that of the binary (y) family. As x increases from 0, the necks grow and the shape elongates, raeching a maximum extension at about $x=0.45$, after which it becomes more compact. The end lobes lose mass monotonically with increasing x as the middle lobe becomes larger and more cylinderlike; at the confluence with the quaternary family, it is nearly cylindrical. The evolution of the four-lobed shapes follows similar trends, although they reach a maximum elongation for $x \simeq 0.67$. The central neck grows monotonically with increasing x, but remains relatively small before growing rapidly between $x \simeq 0.7$ and the confluence point at $x \simeq 0.769$. This rapid growth occurs simultaneously with a rapid decrease of the maximum extension of the shape. The neck radii and maximum extension of the ternary and quaternary saddle points are plotted as functions of x in Fig. 5. The deviation of the calculated results in Figs. 3 and 5 from the known values at $x=0$ and the wiggles in the curves for ternary shapes near $x=0.2$ are a further indication that eight parameters are not a sufficient number to accurately represent the geometry of shapes which are nearly tangent spheres with small necks.

For any of the binary saddle-point shapes, the single unstable normal mode is either an elongation or a combination of an elongation with neck shrinkage, depending on the value of x.[4,6] In Fig.

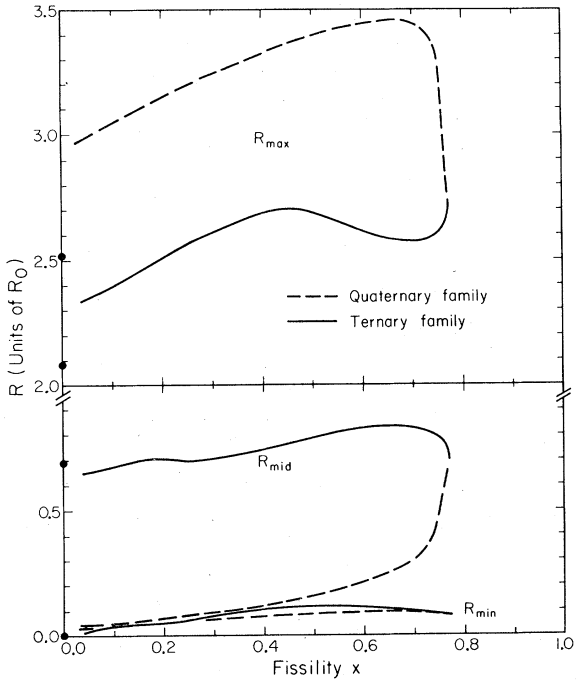

FIG. 5. Half-length, outer neck radius, and central radius as functions of the fissility for the ternary and quaternary saddle points. R_{max} is one-half the maximum length of the shape. R_{mid} is the cylindrical radius at the center of the shape, and R_{min} is the radius of the outer necks. The dots on the $x=0$ axis indicate the properties of three and four equal tangent spheres.

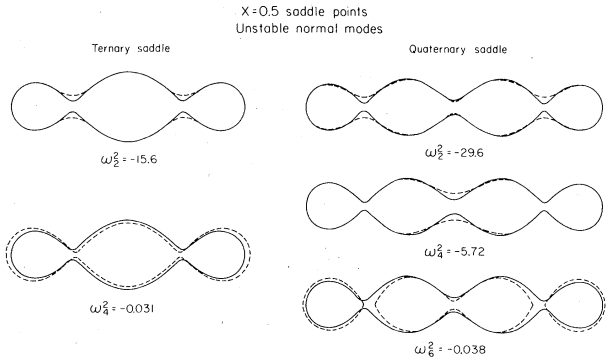

FIG. 6. Unstable normal modes for the $x=0.5$ ternary and quaternary saddle points. The solid lines show the saddle-point shapes while the dashed lines show the shapes when displaced an arbitrary amount along the eigenvector corresponding to the frequency indicated below each shape. The frequencies of the mass-symmetric normal modes are ordered algebraically and labeled in order with even integers.

6, we illustrate the unstable normal modes for the $x=0.5$ ternary and quaternary saddle points. The most unstable mode for both shapes corresponds to a growth or shrinkage of the outside necks and results in little mass transfer between the lobes. The second-most unstable mode of the quaternary shape is a growth or shrinkage of the central neck. The mode is less unstable than the previous mode because the central neck is thicker than the outside ones. For both shapes the least unstable mode corresponds to mass transfer across the outside necks toward or away from the outside lobes.

V. SUMMARY AND CONCLUSION

We have introduced a new parametrization for axially symmetric liquid-drop shapes which is both flexible and easily generalizable. This parametrization is suitable for spherical and nearly spherical shapes, as well as more highly deformed and multi-necked configurations. However, it is somewhat poorer in representing shapes with high-curvature necks, such as tangent spheroids. With this parametrization, we are able to reproduce or improve upon earlier calculations of the properties of binary saddle-point shapes for uniformly charged liquid drops. We are also able to calculate the properties of ternary and quaternary saddle points, which have higher energies and more degrees of instability than the usual binary saddle points.

This parametrization allows, for the first time, a study of the onset of prolate ternary fission in very large systems. Systematic investigations of heavy-ion collisions are also possible. Further refinements which can be incorporated are the inclusion of mass-asymmetric distortions, the effects of various forms of dissipation,[8,20] and the replacement of the liquid-drop surface energy with a macroscopic nuclear energy including the effects of the finite range of the nuclear force.[21]

ACKNOWLEDGMENTS

This work was supported in part by the National Science Foundation under Grants Nos. PHY77-21602 and PHY76-83685 and the U.S. Department of Energy. One of the authors (S.E.K.) gratefully acknowledges support by the Alfred P. Sloan Foundation.

APPENDIX A: ENERGIES, FORCES, AND INERTIAS

In this appendix, we present expressions in our parametrization for the various contributions to the liquid-drop energy, their derivatives with respect to the shape parameters, and the elements of the Werner-Wheeler inertia tensor.

1. Rotational energy

For a reflection-symmetric drop rotating about an axis perpendicular to its symmetry axis, the moment of inertia is

$$I_\perp=\frac{\pi\rho_m}{4}\int_{-z_0}^{z_0}dz\left[\rho_s^4(z)+4z^2\rho_s^2(z)\right], \tag{A1}$$

where ρ_m is the uniform mass density. Utilizing Eq. (7), we find, in dimensionless units,

$$I_\perp=\frac{z_0^2}{3}+\frac{1}{6z_0}+\frac{a_2z_0^3}{5}+\frac{3z_0}{8}\sum_n\frac{a_n^2}{2n+1}. \tag{A2}$$

For rotation about the axis of symmetry, the moment of inertia is

$$I_\parallel=\frac{\pi\rho_m}{2}\int_{-z_0}^{z_0}dz\rho_s^4(z), \tag{A3}$$

which leads to

$$I_\parallel=\frac{1}{3z_0}+\frac{3z_0}{4}\sum_n\frac{a_n^2}{2n+1}. \tag{A4}$$

The dimensionless rotational energy is

$$B_r=\frac{2}{5I}, \tag{A5}$$

so that the computation of the generalized rotational forces requires the derivatives

$$\frac{\partial I_\perp}{\partial a_k}=\frac{3}{4}\frac{z_0a_k}{2k+1}+z_0^3(1+\tfrac{1}{5}\delta_{k2})+\tfrac{9}{10}z_0^4a_2-\tfrac{1}{4}+\tfrac{9}{16}z_0^2\sum_n\frac{a_n^2}{2n+1} \tag{A6a}$$

and

$$\frac{\partial I_\parallel}{\partial a_k}=\frac{3}{2}\frac{z_0a_k}{2k+1}-\frac{1}{2}+\frac{9}{8}z_0^2\sum_n\frac{a_n^2}{2n+1}. \tag{A6b}$$

2. Surface energy

The dimensionless surface energy is simply the surface area of the drop divided by the area of a sphere having the same volume:

$$B_s=\frac{z_0}{2}\int_{-1}^{1}dx\left[u(x)+\left(\frac{u'(x)}{2z_0}\right)^2\right]^{1/2}, \tag{A7}$$

where the prime denotes differentiation with respect to x. The generalized surface forces are

$$\frac{\partial B_s}{\partial a_k}=\frac{3}{2}z_0B_s+\frac{z_0}{4}\times\int_{-1}^{1}dx\,\frac{[\partial u/\partial a_k-3u'^2/4z_0+u'(\partial u'/\partial a_k)/2z_0^2]}{(u+u'^2/4z_0^2)^{1/2}}, \tag{A8}$$

with

$$\frac{\partial u(x)}{\partial a_k}=P_k(x)-1, \tag{A9a}$$

$$u'(x)=\sum_n a_nP_n'(x), \tag{A9b}$$

and

$$\frac{\partial u'(x)}{\partial a_k}=P_k'(x), \tag{A9c}$$

all following from Eq. (7). We evaluate the integrals in Eqs. (A7) and (A8) with Gauss-Legendre quadrature formulas. Lengthy analytic expressions for the second derivatives $\partial^2B_s/\partial a_j\partial a_k$ can also be derived.

3. Coulomb energy

Using Eq. (3.4) of Ref. 22 we may express the dimensionless Coulomb energy as

$$B_c=\frac{5z_0^2}{24\pi}\int_{-1}^{1}dx\int_{-1}^{1}dx'I_c, \tag{A10}$$

where

$$I_c=\{[K(k)-2D(k)]F_1+K(k)F_2\}/D_1^{1/2}, \tag{A11}$$

$$D(k)=[K(k)-E(k)]/k^2, \tag{A12}$$

$K(k)$ and $E(k)$ are complete elliptic integrals of the first and second kinds, respectively, and where

$$k^2=4G_1/D_1, \tag{A13a}$$

$$G_1=[u(x)u(x')]^{1/2}, \tag{A13b}$$

$$D_1=z_0^2\Delta x^2+u(x)+u(x')+2G_1, \tag{A13c}$$

and

$$\Delta x=x-x'. \tag{A13d}$$

The two auxiliary functions F_1 and F_2 are defined by

$$F_1=G_1\{2u(x)+2u(x')+\tfrac{3}{2}\Delta x[u'(x')-u'(x)]-z_0^2\Delta x^2\} \tag{A14a}$$

and

$$F_2=4G_1^2+\tfrac{3}{2}\Delta x[u(x)u'(x')-u'(x)u(x')-\tfrac{1}{2}\Delta x\,u'(x)u'(x')]. \tag{A14b}$$

The generalized Coulomb force is

$$-\frac{\partial B_c}{\partial a_k}=-3z_0B_c-\frac{5z_0^2}{24\pi}\int_{-1}^{1}dx\int_{-1}^{1}dx'\frac{\partial I_c}{\partial a_k} \tag{A15}$$

and analytic formulas for the integrand can be derived by differentiating Eqs. (A11) through (A14). Although lengthy expression for the second derivatives of the Coulomb energy $\partial^2B_c/\partial a_j\partial a_k$ can

be readily derived, in this work the second derivatives are evaluated by numerically differentiating (A15). The integrals in (A10) and (A15) are evaluated by Gauss-Legendre quadrature.

4. Inertia tensor

In order to calculate the normal-mode frequencies and eigenvectors at an equilibrium shape, we need the inertia tensor in addition to the second derivatives of the potential energy. To keep the calculation of the inertia relatively simple, we use the Werner-Wheeler approximation to incompressible, irrotational flow to specify the fluid velocity field in terms of the time derivatives of the generalized coordinates $\{\dot{a}_n\}$.[6,8] In this approximation for axially symmetric systems, the cylindrical components of the fluid velocity $\vec{v}$ are

$$v_\varphi = 0\,, \tag{A16a}$$

$$v_z(z) = \sum_n \dot{a}_n A_n(z,a)\,, \tag{A16b}$$

$$v_\rho(\rho,z) = -\frac{\rho}{2}\sum_n \dot{a}_n \frac{\partial A_n}{\partial z}(z,a)\,, \tag{A16c}$$

where

$$A_n = \frac{1}{\rho_s^2(z)}\frac{\partial}{\partial a_n}\int_z^{z_0} \rho_s^2(z')dz'\,. \tag{A17}$$

From our expansion (7) we find

$$A_n(z) = \tfrac{3}{2} z_0^2\left[x + \frac{1}{u(x)}\sum_m \frac{(a_m + 2\delta_{nm}/3z_0)}{2m+1} \times [P_{m-1}(x) - P_{m+1}(x)]\right] \tag{A18}$$

and

$$A_n'(x) \equiv \frac{\partial A_n}{\partial z} = \frac{1}{u(x)}\left[1 - P_n(x) + \tfrac{3}{2} z_0 u'(x)[x - 2A_n(x)/3z_0^2]\right]. \tag{A19}$$

In terms of the $\{A_n\}$ and their derivatives, the kinetic energy T is

$$T = \frac{\rho_m}{2}\int d^3r\, v^2 = \tfrac{1}{2}\sum_{ij} \dot{a}_i M_{ij} \dot{a}_j \tag{A20}$$

and the inertia tensor is

$$M_{ij} = \tfrac{3}{4} z_0 \int_{-1}^{1} dx\, u(x)\left[A_i(x)A_j(x) + \frac{u(x)}{8} A_i'(x)A_j'(x)\right]. \tag{A21}$$

APPENDIX B: ACCURACY OF THE CALCULATIONS

We evaluate Eqs. (A7), (A8), (A10), (A15), and and (A21) by means of Gauss-Legendre quadrature. Our standard evaluation uses 32-point formulas over the interval $[-1, 1]$. For increased

TABLE II. Convergence of selected quantities with quadrature order. Calculated values of the surface and Coulomb energies, one element of the inertia tensor, and one component of the surface and Coulomb force vectors for four different shapes, using different values of Q, the number of Gaussian quadrature points. The numbers were calculated on a CDC 7600 computer which has a word length corresponding to about 14 digits, and were printed out with 12 figures to the right of the decimal point.

Shape	Q	B_s	B_c	M_{22}	$\partial B_s/\partial a_2$	$\partial B_c/\partial a_2$
Sphere	32	$1.0+0\times10^{-12}$	$1.0+3\times10^{-9}$	0.675 000 ...	$<5\times10^{-13}$	-3×10^{-9}
	64	$1.0+0\times10^{-12}$	$1.0+2\times10^{-10}$	0.675 000 ...	$<5\times10^{-13}$	-1×10^{-10}
	128	$1.0+0\times10^{-12}$	$1.0+1\times10^{-11}$	0.675 000 ...	$<5\times10^{-13}$	$<5\times10^{-13}$
	256	$1.0+0\times10^{-12}$	$1.0+1\times10^{-12}$	0.675 000 ...	$<5\times10^{-13}$	1×10^{-12}
$x=0.3$	32	1.274 741 36	0.823 808 45	18.128 305	0.520 312 01	−0.775 901 59
binary	64	1.273 628 74	0.823 806 74	18.122 580	0.465 627 84	−0.776 044 55
saddle	128	1.273 628 74	0.823 806 73	18.122 580	0.465 627 85	−0.776 044 58
point	256	1.273 628 74	0.823 806 73	18.122 580	0.465 627 85	−0.776 044 59
$x=0.3$	32	1.457 268 13	0.740 856 55	60.819	0.948 058	−1.262 378 5
ternary	64	1.456 432 63	0.740 848 54	60.192	0.856 167	−1.262 496 6
saddle	128	1.455 857 63	0.740 848 00	60.323	0.756 781	−1.262 568 5
point	256	1.455 868 97	0.740 847 99	60.333	0.762 278	−1.262 568 6
$x=0.3$	32	1.615 433 10	0.671 007 30	144.366	1.530 33	−1.611 562
quaternary	64	1.607 639 04	0.670 946 01	148.403	0.897 94	−1.613 691
saddle	128	1.608 550 04	0.670 946 21	146.454	0.982 98	−1.613 588
point	256	1.608 567 04	0.670 946 21	146.501	0.989 76	−1.613 588

accuracy, we may divide this interval into 2, 4, or 8 equal subintervals and use the 32-point formula in each, thus generating 64-, 128-, and 256-point formulas, respectively. For selected shapes with $N=8$, we show in Table II how the energies, one element of the inertia tensor, and selected force components vary with increasing quadrature order. (Except for isolated special cases, all Coulomb or surface force components for a particular shape are of comparable magnitude.)

For a sphere, or nearly spherical shape, 32 quadrature points ($Q=32$) provide sufficient accuracy (error $\lesssim 10^{-8}$). For a typical, moderately deformed y family shape, such as the $x=0.3$ case shown, $Q=64$ is necessary. For the more highly deformed ternary and quaternary shapes, the surface energy, surface forces, and inertia tensor are the least accurately computed quantities, despite the fact that only a one-dimensional integral is required for their evaluation. All the calculations in this paper used $Q=64$ for the Coulomb energy and its derivatives while $Q=128$ was used for the inertia tensor elements and the surface energy and forces. Note that while the error in the Coulomb derivative for the quaternary shape is about 1×10^{-4} for $Q=64$, the error in the surface-energy derivative is about 7×10^{-3} for $Q=128$.

---

*Permanent address.

[1]N. Bohr and J. A. Wheeler, Phys. Rev. 56, 426 (1939).
[2]D. L. Hill and J. A. Wheeler, Phys. Rev. 89, 1102 (1953).
[3]W. J. Swiatecki, Phys. Rev. 104, 993 (1956).
[4]S. Cohen and W. J. Swiatecki, Ann. Phys. (N.Y.) 22, 406 (1963).
[5]J. N. P. Lawrence, Phys. Rev. 139, B1227 (1965); Ph.D. thesis, Los Alamos Scientific Laboratory Report LA-3774 (1967).
[6]J. R. Nix, Nucl. Phys. A130, 241 (1969); Lawrence Berkeley Laboratory Report No. UCRL-17958, 1968 (unpublished).
[7]S. Cohen, F. Plasil, and W. J. Swiatecki, Ann. (N.Y.) 82, 562 (1974).
[8]K. T. R. Davies, A. J. Sierk, and J. R. Nix, Phys. Rev. C 13, 2385 (1976).
[9]C. T. Alonso, in *Proceedings of the International Colloquium on Drops and Bubbles, Pasadena, 1974,* edited by D. J. Collins, M. S. Plesset, and M. M. Saffren (California Institute of Technology, Pasadena, 1976), Vol. I, p. 139.
[10]A. J. Sierk and J. R. Nix, in *Proceedings of the Third International Atomic Energy Symposium on the Physics and Chemistry of Fission, Rochester, 1973* (International Atomic Energy Agency, Vienna, 1974), Vol. II, p. 273.
[11]A. J. Sierk and J. R. Nix, Phys. Rev. C 16, 1048 (1977).
[12]A. J. Sierk (unpublished).
[13]J. R. Nix, Ann. Phys. (N.Y.) 41, 52 (1967).
[14]W. J. Swiatecki, Proceedings of the Second United Nations International Conference on the Peaceful Uses of Atomic Energy, paper P/651 (1958), p. 248.
[15]T. Johansson, S. G. Nilsson, and Z. Szymanski, Ann. Phys. (Paris) 5, 377 (1970).
[16]R. W. Hasse, Ann. Phys. (N.Y.) 68, 377 (1971).
[17]M. Brack, J. Damgaard, H. C. Pauli, A. S. Jensen, V. M. Strutinsky, and C. Y. Wong, Rev. Mod. Phys. 44, 320 (1972).
[18]U. Mosel and H. W. Schmitt, Nucl. Phys. A165, 73 (1971).
[19]V. M. Strutinsky, N. Ya. Lyaschenko, and N. A. Popov, Zh. Eksp. Teor. Fiz. 43, 584 (1962) [Sov. Phys.—JETP 16, 418 (1963)]; Nucl. Phys. 46, 639 (1963).
[20]J. Blocki, Y. Boneh, J. R. Nix, J. Randrup, M. Robel, A. J. Sierk, and W. J. Swiatecki, Ann. Phys. (N.Y.) 113, 330 (1978).
[21]H. J. Krappe, J. R. Nix, and A. J. Sierk, Phys. Rev. Lett. 42, 215 (1979).